Copper-Intercalated Birnessite as a Water Oxidation Catalyst

Akila C. Thenuwara,[†,§] Samantha L. Shumlas,[†,§] Nuwan H. Attanayake,[†,§] Elizabeth B. Cerkez,[†] Ian G. McKendry,[†,§] Laszlo Frazer,[†,§] Eric Borguet,[†,§] Qing Kang,[†,§] Michael J. Zdilla,[†,§] Jianwei Sun,[‡,§] and Daniel R. Strongin*,[†,§]

[†]Department of Chemistry, Temple University, Beury Hall, 1901 North 13th Street, Philadelphia, Pennsylvania 19122, United States

[‡]Department of Physics, Temple University, 1925 North 12th Street, Philadelphia, Pennsylvania 19122, United States

[§]Center for Computational Design of Functional Layered Materials (CCDM), Temple University, Philadelphia, Pennsylvania 19122, United States

S *Supporting Information*

ABSTRACT: We report a synthetic method to increase the catalytic activity of birnessite toward water oxidation by intercalating copper in the interlayer region of the layered manganese oxide. Intercalation of copper, verified by XRD, XPS, ICP, and Raman spectroscopy, was accomplished by exposing a suspension of birnessite to a Cu^+-bearing precursor molecule that underwent disproportionation in solution to yield Cu^0 and Cu^{2+}. Electrocatalytic studies showed that the Cu-modified birnessite exhibited an overpotential for water

oxidation of ~490 mV (at 10 mA/cm^2) and a Tafel slope of 126 mV/decade compared to ~700 mV (at 10 mA/cm^2) and 240 mV/decade, respectively, for birnessite without copper. Impedance spectroscopy results suggested that the charge transfer resistivity of the Cu-modified sample was significantly lower than Cu-free birnessite, suggesting that Cu in the interlayer increased the conductivity of birnessite leading to an enhancement of water oxidation kinetics. Density functional theory calculations show that the intercalation of Cu^0 into a layered MnO_2 model structure led to a change of the electronic properties of the material from a semiconductor to a metallic-like structure. This conclusion from computation is in general agreement with the aforementioned impedance spectroscopy results. X-ray photoelectron spectroscopy (XPS) showed that Cu^0 coexisted with Cu^{2+} in the prepared Cu-modified birnessite. Control experiments using birnessite that was decorated with only Cu^{2+} showed a reduction in water oxidation kinetics, further emphasizing the importance of Cu^0 for the increased activity of birnessite. The introduction of Cu^0 into the birnessite structure also increased the stability of the electrocatalyst. At a working current of 2 mA, the Cu-modified birnessite took ~3 times longer for the overpotential for water oxdiation to increase by 100 mV compared to when Cu was not present in the birnessite.
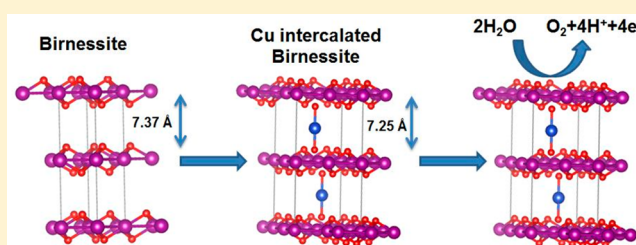
1. INTRODUCTION

The water oxidation reaction is central to solar energy driven fuel producing reactions such as hydrogen evolution and carbon dioxide reduction.[1,2] Thermodynamically, the reaction requires 1.23 V (at pH = 0),[3] but in reality due to sluggish kinetics it is usually accompanied by a large overpotential (η).[4] Precious metals such as Ru and Ir and their oxides have been identified as excellent water oxidation catalysts; however, implementation of these catalysts in commercial water oxidation devices has been restricted due to the cost and scarcity of these materials. Hence, development of cheaper and nonprecious metal bearing catalysts is an area of intense study. First row transition metal (Ni, Co, Fe, and Mn) oxides and their hydroxides have been identified as possible candidates for catalyzing water oxidation due to their earth abundance, moderate activity, and stability.[1,5−7] Recent studies have also investigated transition metal chalcogenides,[8,9] phosphates,[3,10] and perovskites[11] as water oxidation catalysts.

Recently, much attention has been given to birnessite (e.g., δ-MnO_2) as a moderately active water oxidation catalyst due to its high abundance, low cost, and low environmental impact. The oxygen evolving complex in photosystem II (PSII) is also composed of a cluster containing Mn and Ca, and thus the study of manganese oxides in general may help shed light on a process that nature has perfected.[12] Manganese oxides can also serve as bifunctional electrocatalysts which can perform oxygen evolution as well as oxygen reduction in alkaline media.[13] However, the catalytic activity of manganese oxide is significantly lower than Ru-, Ir-, Ni-, and Co-bearing systems.

The enhancement of the catalytic activity of cheap, abundant materials without the introduction of expensive, rare materials is a worthwhile goal. Toward this end, prior studies have focused on enhancing the water oxidation activity of manganese oxides—albeit with limited success—through synthetic strategies that have included doping, coating with metals, and integrating the material with conductive nanostructures.[14−16] A

number of studies have theoretically and experimentally suggested that the presence of Mn^{3+} plays a key role in manganese oxide based catalytic systems, though a definitive explanation for this experimental observation is still lacking.[13,17−19] Dismukes and co-workers showed by investigating the water oxidation kinetics on a variety of manganese oxides in the presence of photoexcited $[Ru(bpy)_3]^{2+}$ that those materials containing greater proportions of Mn^{3+} (e.g., Mn_2O_3) had a higher activity than those with higher proportions of Mn^{4+} (e.g., birnessite) in the crystal structure.[20] The weaker Mn^{3+}−O bond (relative to Mn^{4+}−O) and longer Mn−Mn bonds lead to a more catalytically viable chemical environment. Suib and co-workers subsequently showed that the electrocatalytic oxidation of water also occurred more readily on the Mn^{3+}-bearing manganese oxides than on δ-MnO_2.[21] These experimental observations are also consistent with the unique activity of Mn^{3+} sites, and these studies also show that the charge transfer resistance was significantly lower for the more active manganese oxide compounds than for birnessite.[4,21] Hence, the water oxidation activity of birnessite may be compromised by poor electrical properties that impede charge flow that is critical for an efficient water oxidation catalyst. This higher resistance could conceivably be in part due to the structure of birnessite, which features octahedrally coordinated manganese arranged in sheets, and held together by relatively weak interlayer forces. Therefore, it might be expected that electrical conductivity between these octahedral sheets (out-of-plane) during water catalysis is limited relative to conductivity within the plane of a particular sheet.

A hypothesis tested in the present research is that the intercalation of metal into the interlayer region of birnessite will lower the charge transfer resistance and increase the catalytic activity during water oxidation chemistry. An approach to test this hypothesis is provided by recent research by Motter et al. that developed a general strategy to intercalate zerovalent metals (e.g., Cu, Au, and Ni) into layered nanomaterials (such as Sb_2Te_3, GaSe, and MoO_3). In this prior study, Cu was shown to intercalate into the layered material during its exposure to a Cu^+ precursor that underwent a disproportionation reaction to produce Cu^0 and Cu^{2+} in an organic (i.e., acetone) medium.[22] It was shown that materials such as Sb_2Te_3 could accommodate interlayer Cu intercalation levels up to 50 at. %, while a layered material such as MoO_3 accommodated up to about 10 at. % Cu.

In this contribution we show, primarily based on X-ray diffraction (XRD) and X-ray photoelectron spectroscopy (XPS) that by using the synthetic protocol described previously, zerovalent copper (coexisting with Cu^{2+}) can be introduced into the interlayer region of birnessite. Electrochemical studies show that the presence of Cu^0 in the interlayer region leads to an enhanced activity and stability of birnessite in the context of water oxidation chemistry. In particular, the overpotential for water oxidation is reduced from 700 to 490 mV (at a current of 10 mA/cm^2) in the presence of interlayer Cu. Impedance spectroscopy measurements indicate that the charge transfer resistance is reduced by 50% when Cu^0 is present, suggesting that Cu^0 increases the conductivity of the layered material. Density functional theory calculations support this experimental observation and show that the intercalation of Cu^0 into a layered model birnessite structure leads to the evolution of states at the Fermi level, and thus a change of the electronic properties of the material from semiconducting toward metallic behavior.

2. EXPERIMENTAL SECTION

2.1. Materials and Methods. All of the chemicals used in this study were purchased from commercial vendors and used without further purification. XRD data were acquired on a Bruker Kappa APEX II DUO diffractometer using Mo Kα radiation from a sealed molybdenum tube with a TRIUMPH monochromator. XPS of the dry samples were collected with Thermo Scientific K-alpha+ at the University of Delaware. Transmission electron microscopy (TEM) images were collected using a JEOL JEM-1400 microscope operating at 120 kV. Scanning electron microscopy (SEM) images were obtained using a FEI Quanta 450 FEG-SEM microscope operating at 30 kV. Energy dispersive spectroscopy (EDS) analysis was performed by an Oxford systems nanoanalysis EDS system, using Aztec 2.1 as the analyzing software. Elemental analysis was performed using a Thermo Scientific iCAP 7000 Series inductively coupled plasma optical emission spectrometer (ICP-OES). Raman measurements were performed using a Horiba Labram HR800 Evo confocal Raman spectrometer with 532 nm excitation and a 100× objective. The resolution of the Raman spectrometer is about 3 cm^{-1}. The excitation laser intensity was maintained below the sample optical damage threshold. All samples were pressed into pellets to obtain a smooth surface for Raman analysis.

2.1.1. Synthesis of Birnessite with and without Copper. Four different samples were used in this study: (1) synthetic birnessite, (2) birnessite exposed to a Cu^+-precursor molecule in acetone, (3) birnessite exposed to Cu^{2+} in acetone, and (4) birnessite that was synthesized in the presence of aqueous Cu^{2+}. Synthesis details for each case are as follows.

Synthetic Birnessite. Following the protocol of McKenzie,[23] potassium−birnessite was made by adding hydrochloric acid (HCl, 4 M, 50.0 mL) dropwise via a syringe pump at 1 mL/min to a heated and stirred (80 °C, 360 rpm) solution of potassium permanganate ($KMnO_4$, 0.200 M, 250 mL) in a 400 mL beaker. Heating continued at 80 °C for an additional 0.5 h after the addition of the acid was complete. The resulting 300 mL solution was then covered to prevent excessive evaporation overnight and aged for 15 h at 50 °C before being washed five times via vacuum filtration with a fine frit to give layered manganese oxide. XRD was used to confirm the existence of postassium−birnessite. The structure of potassium−birnessite resulting from this synthetic protocol is characterized by cation vacancies in the octahedral sheets with $Mn^{3+/2+}$ in the interlayer region.[24]

Copper(I)−Birnessite. This sample was prepared by exposing 0.200 g of the prepared birnessite described previously to 0.192 g of tetrakis(acetonitrile)copper(I) hexafluorophosphate in acetone. The mixture was refluxed at 45 °C for 4 h, and the resulting powder was vacuum-filtered and washed with excess acetone and ethanol. Prior research has shown that tetrakis(acetonitrile)copper(I) hexafluorophosphate undergoes slow disproportionation to Cu^0 and Cu^{2+} in acetone.[22] Hence, this synthetic protocol exposed birnessite to both Cu^0 and Cu^{2+}.

Copper(II)−Birnessite. As a control sample, birnessite was refluxed in acetone at 45 °C, but unlike the preparation of copper(I)−birnessite, this particular sample was exposed to a solution of Cu^{2+} [10 mM $Cu(NO_3)$]. This Cu-modified sample was vacuum-filtered and washed with excess acetone and ethanol.

Copper(II)-Doped Birnessite. Finally, a third Cu^{2+}-modified birnessite sample was synthesized by introducing Cu^{2+} [1 mM $Cu(NO_3)$] into a solution containing potassium permanganate ($KMnO_4$, 0.200 M, 250 mL) in a 400 mL beaker. HCl (4 M, 50.0 mL) was added dropwise to the $Cu^{2+}/KMnO_4$ solution (80 °C) via a syringe pump at a rate of 1 mL/min. The temperature of the reaction cell was maintained at 80 °C for an additional 0.5 h after addition was completed. The resulting Cu-modified sample was washed with water and dried via lyophilization.

2.2. Computational Details. All calculations were performed by the Vienna ab initio simulation package (VASP)[25] using periodic density functional theory (DFT). The projector augmented wave (PAW) method was used to describe valence-electron interactions. The newly developed strongly constrained and appropriately normed

(SCAN) meta-generalized gradient approximation (metaGGA)[26] was used for the exchange-correlation energy. The layered manganese dioxide was modeled as a crystal of MnO_2 with a space group $P6_3/mmc$. Two copper atoms were then intercalated between layers of the $2 \times 2 \times 1$ unit cell with each Cu directly connecting two oxygen atoms of different layers. The positions of Cu were chosen such that they were in different interlayers and as far away from each other as possible (see Supporting Information (SI) Figures S1 and S2). The energy cutoff was set to 520 eV, and electron smearing was employed using a Gaussian smearing technique with a width of 0.05 eV. Spin polarization calculations were carried out, and antiferromagnetic configurations were used for all of the calculations. Electronic energies were computed with the self-consistent field (SCF) tolerance of 10^{-5} eV, and total forces were converged to less than 0.01 eV/Å. The energy integrations were performed in the first Brillouin zone with a γ-centered $12 \times 12 \times 4$ k mesh for the bulk layered MnO_2 and $3 \times 3 \times 2$ for the Cu^0-intercalated MnO_2.

2.3. Electrochemical Characterization. Electrochemical water oxidation of birnessite and Cu-modified birnessite was carried out in an alkaline medium (1 M KOH) in a standard three-electrode system using an Ag/AgCl reference electrode and Pt wire as the counter electrode. The oxygen evolution reaction (OER) was studied using cyclic voltammetry (CV) and liner sweep voltammetry (LSV) using a CHI 660E electrochemical workstation at ambient temperature (22 ± 2 °C). The working electrode was prepared by drop casting 20 μL of catalyst ink solution on a 3 mm diameter glassy carbon (GC) electrode (loading, 0.82 mg/cm^2). The ink solution was prepared as follows: 3 mg of catalyst and 7 mg of carbon (VulcanXC-72) were dispersed in 1 mL of isopropanol and sonicated for 3 min, followed by adding 35 μL of Nafion solution (5% in alcohol; Ion Power Inc.). The resulting mixture was sonicated for 60 min to form a suspension. All of the polarization curves were recorded at a 5 mV/s scan rate. For all of the catalysts tested here, polarization curves were replicated 5 times and the overpotential (to produce 10 mA/cm^2) and Tafel slopes reported are based on an analysis of these data.

3. RESULTS AND DISCUSSION

3.1. Characterization of Copper-Intercalated Birnessite. Figure 1 exhibits SEM and TEM micrographs showing the
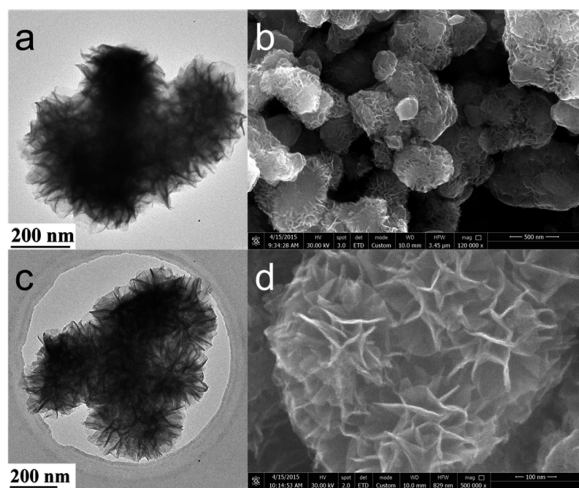

Figure 1. Electron microscopy images of birnessite: (a) TEM and (b) SEM. Images of copper(I)−birnessite: (c) TEM and (d) SEM.

morphology of birnessite before and after exposure to Cu^0 (i.e., copper(I)−birnessite). Typical potassium−birnessite is composed of a flower-like microsphere nanostructure which is retained after Cu-modification. Both EDS (Figure S6) and ICP-OES confirmed that the concentration of Cu in copper(I)−birnessite is ∼2 at. %. Two experimental observations suggest

that at least a fraction of the Cu was located within the interlayer region. XRD of copper(I)−birnessite and Cu-free birnessite indicated that birnessite exposed to Cu^0 led to shifts in the (001) and (002) Bragg reflections toward higher 2θ indicating a contraction of the interlayer spacing (Figure 2).

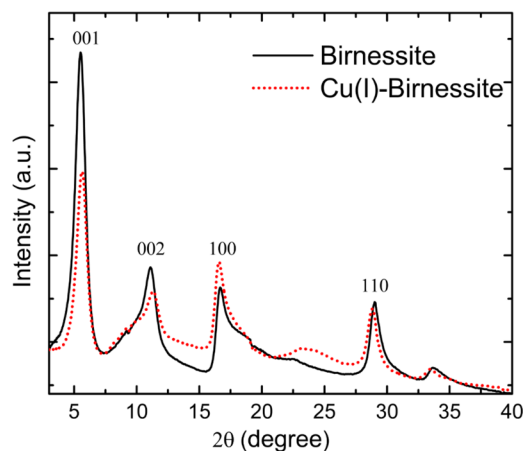**Figure 2.** XRD patterns of birnessite and copper(I)−birnessite which indicates the shift in Bragg reflections toward higher 2θ signifying a contraction of the interlayer spacing.

This experimental observation is consistent with prior studies that showed similar shifts in Bragg reflections after the intercalation of zerovalent metal into the interlayer region of layered compounds.[22,27,28] No such shift is observed in the XRD associated with copper(II)−birnessite and Cu(II)-doped birnessite (SI Figure S11). Based on the shift of the (001) reflection observed for copper(I)−birnessite, the interlayer spacing decreased from 7.37 to 7.25 Å upon Cu addition, suggesting that the Cu resides in the interlayer region. Further characterization via Raman spectroscopy (Figure 3) suggests that there is some disordering of the octahedral sheets when birnessite is exposed to the Cu(I) precursor. Cu-free birnessite exhibits two primary Raman features at 575 cm^{-1} (in-plane symmetric stretching of the Mn−O bond) and at 646 cm^{-1} (out-of-plane symmetric stretching of Mn−O of MnO_6 groups).[29] In Figure 3, both copper(I)−birnessite and copper-
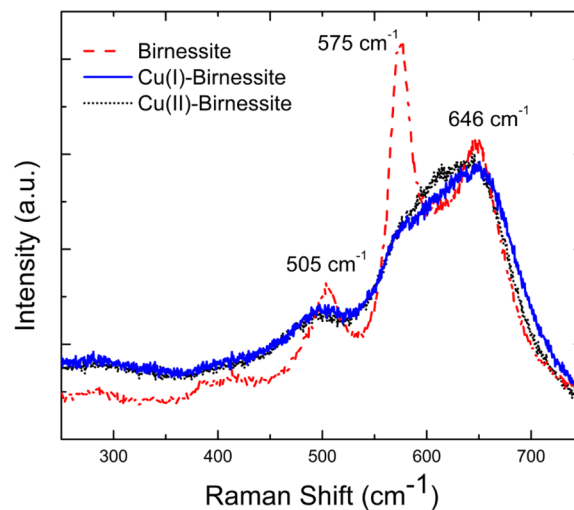

Figure 3. Raman spectra of birnessite, copper(II)−birnessite, and copper(I)−birnessite.

(II)−birnessite exhibit similar Raman spectra where the Mn−O stretching mode shows significant broadening or weakening relative to the out-of-plane mode, possibly indicating some disruption of the Mn−O bonding in the sheets. SI Figure S9 shows the gradual, consistent evolution of the Raman spectrum with copper concentration. The similarity between the copper(I)− and copper(II)−birnessite data suggests that Cu(II) on the mineral surface (and not in the interlayer region) is the main contributor to the disordering. Cu^0 in the interlayer are likely not contributing to the disordering and only to the change in the interlayer distance.

Cu 2p XPS data, exhibited in Figure 4, indicate that Cu^0 exists along with Cu^{2+} in the structure of copper(I)−birnessite.
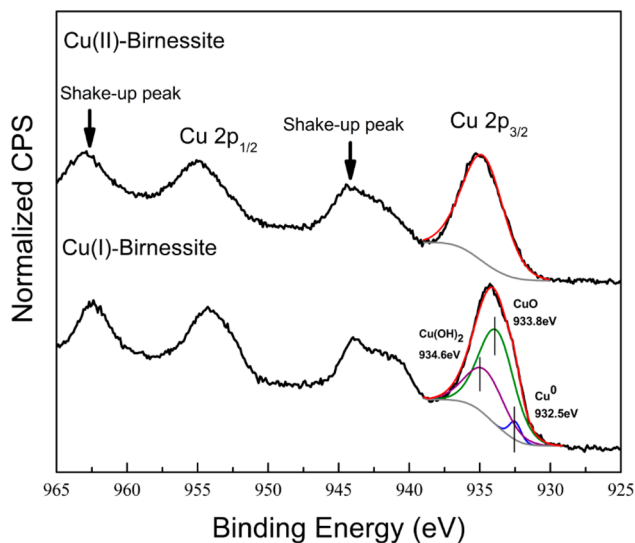

Figure 4. Cu 2p XPS of copper(I)−birnessite and copper(II)−birnessite. The spectra are fitted with three peaks corresponding to Cu^0 (blue curve), CuO (green curve), and $Cu(OH)_2$ (purple curve). The black curve corresponds to the raw data, and the red curve corresponds to the simulated curve after the peak fitting process.

The presence of well-defined shake up peaks in the 940−946 eV region, similarly observed in copper oxides (Cu^{2+}), verifies the presence of Cu^{2+} in copper(I)−birnessite, although we cannot rule out that Cu^{2+} is the result of exposing the sample to air prior to analysis. The copper(I)−birnessite spectrum also contains spectral weight consistent with the presence of Cu^0. We also present Cu 2p XPS of copper(II)−birnessite, and as anticipated the spectra (Figure 4) show the characteristic satellite peak structure characteristic of copper oxides. Based on the spectral fitting of the Cu $2p_{3/2}$ peak in the copper(I)−birnessite spectrum, we estimate that 4.1% Cu^0, 63.1% CuO, and 32.8% $Cu(OH)_2$ contribute to the Cu 2p peak. Analysis of the fitted Cu $2p_{3/2}$ peak for copper(II)−birnessite shows that all of the spectral weight is due to $Cu(OH)_2$ where a significant amount of the Cu^{2+} in the copper(I)−birnessite is due the

oxidation of Cu^0 to Cu^{2+} in the interlayer region. We support this assignment with two experimental observations. First, when birnessite is exposed to only Cu^{2+} in solution, there is significant K^+ loss from the interlayer region (see Table 1). Second, in contrast we find significantly less K^+ is lost from the interlayer region when birnessite is modified to form copper(I)−birnessite. Our interpretation is that the introduction of Cu^{2+} directly into the interlayer region via diffusion from solution displaces K^+ from the interlayer due to charge-neutrality considerations. In contrast, the diffusion of charge-neutral Cu^0 (resulting from the disproportionation of the Cu(I) reagent) into the interlayer region can occur without K^+ displacement. This line of reasoning leads to the conclusion that some portion of the Cu^0 in the interlayer is oxidized to Cu^{2+}, presumably with the concomitant reduction of a stoichiometric amount of Mn(IV) and/or Mn(III) in the octahedral sheets. To investigate possible changes in Mn valency, we acquired and compared Mn 2p XPS data for copper(I)−birnessite and Cu-free birnessite (see SI Figure S4), but found no discernible difference. We add, however, that the maximum amount of Mn that could change oxidation state due to redox chemistry is ∼4% and such a change would be difficult to resolve in the XPS measurement.

3.2. DFT Study of Copper(I)−Birnessite. First-principles density functional theory (DFT) calculations were employed to investigate the effect of Cu intercalation on the electronic properties of copper(I)−birnessite. The structure of pristine birnessite was modeled as layers of MnO_2, each layer of which is composed of MnO_6 octahedra (SI Figure S1). Placement of Cu into the interlayer region was also carried out to model the copper(I)−birnessite system (SI Figure S2). SI Figure S3 exhibits density of states (DOS) plots determined by SCAN. Importantly, DOS plots of copper(I)−birnessite show Mn 3d derived states at the Fermi level (0 eV energy) suggesting that hybridization of the d-levels of Cu and Mn result in a more metallic-like DOS compared to Cu-free birnessite. Intercalated Cu also has an effect on the geometric structure of MnO_2. Cu in the interlayer binds to its closest oxygen atoms, resulting in the dilation of the bond length of the oxygen with its nearest Mn neighbors from 1.894 to 1.931 Å (SI Table S1). This result from calculation is consistent with our experimental observation from Raman spectroscopy that disorder appears in the vibrational spectrum upon Cu addition (SI Figure S9). Charge density plots also suggest that the intercalated Cu^0 is partially oxidized suggesting that Mn in the octahedral sheets is reduced. Finally, while the intercalation of Cu^0 has little effect on the geometry of each individual layer, there is an expansion of the interlayer region upon Cu intercalation by about 1.3 Å. XRD of our samples conversely suggested that the introduction of Cu led to a contraction of the interlayer distance. We emphasize, however, that the model structures do not include interlayer water, which is present in the samples that were analyzed by XRD. Hence, the difference in the interlayer environment

Table 1. Summary of Catalytic Activities and Atomic Ratios from ICP-OES and EDS

catalyst	K/Mn atomic ratio	Cu/Mn atomic ratio	TOF (s^{-1}) at η = 0.45 V	mass activity (A g^{-1}) at η = 0.45 V	Tafel slope (mV dec^{-1})
birnessite	0.10	0.00	0.0004	1.92	243
copper(I)−birnessite	0.09	0.10	0.003	10.24	126
copper(II)−birnessite	0.05	0.13	0.0006	2.57	233
copper(II)-doped birnessite	0.06	0.14	0.0004	1.37	285

between theory and experiment precludes any direct comparison in this regard.

3.2. Electrocatalytic Measurements. Figure 5 exhibits polarization curves for copper(I)−birnessite, copper(II)−
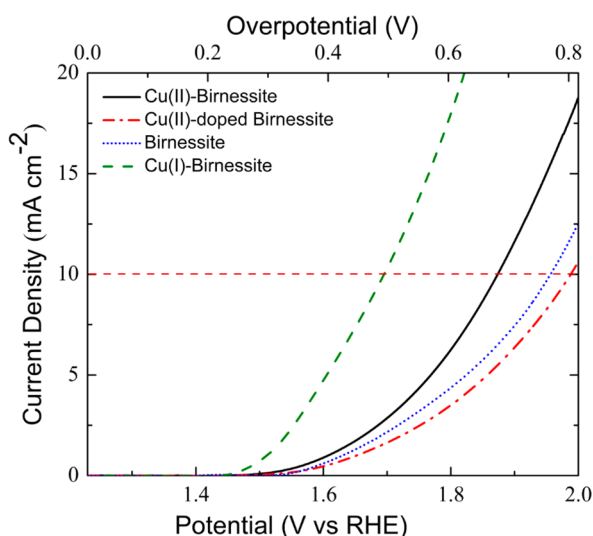

Figure 5. Polarization curves for birnessite and Cu-modified birnessite samples. Copper(I)−birnessite shows a lower overpotential for water oxidation than the other materials. The experiments were carried out in 1 M KOH.

birnessite, Cu(II)-doped birnessite, and Cu-free birnessite. Inspection of these data show that copper(I)−birnessite is the best oxygen evolution catalyst among all of the samples measured. For example, to reach a current of 10 mA/cm², copper(I)−birnessite requires 490 ± 6 mV of overpotential, a decrease of more than 200 mV with respect to Cu-free birnessite. We mention that this overpotential of 490 mV (at 10 mA/cm²) is the lowest overpotential reported in the literature for birnessite. Furthermore, the overpotential measured for copper(I)−birnessite is similar to the value (490 mV) that has been reported for α-MnO$_2$, which is considered to be the most active manganese oxide among all of the polymorphs of MnO$_2$.[4] In addition, the superiority of copper(I)−birnessite with respect to other catalysts studied in this contribution is highlighted by a comparison of Tafel slopes (SI Figure S5). In particular a Tafel slope of 126 ± 3 mV/decade is associated

with copper(I)−birnessite while the other Cu-modified birnessite and Cu-free birnessite exhibit Tafel slopes ∼240 mV/decade (similar to the literature value for birnessite).[4] The experimental observation that copper(II)−birnessite, Cu(II)-doped birnessite, and birnessite all exhibit similar Tafel slopes suggest that the mechanism of water oxidation is similar on all of these surfaces, but dissimilar to copper(I)−birnessite.

The improved catalytic activity of copper(I)−birnessite is also illustrated by a comparison of turnover frequencies (TOF) and mass activities for the different birnessite samples (see Table 1). Copper(I)−birnessite exhibits a water oxidation TOF (at η = 0.45 V) that is 6.8 times higher than Cu(II)-doped birnessite and 4.6 times higher than copper(II)−birnessite (TOF for Cu-free birnessite agrees well with the literature).[4] Prior studies have shown that the stability of birnessite under water oxidation conditions is less than that observed for nonlayered manganese oxides such as Mn$_2$O$_3$. The reason for this is not well understood, but we find that copper(I)−birnessite exhibits a significant improvement in stability relative to Cu-free birnessite, based on chronopotentiometry measurements (Figure 6) for two different current densities: 2 and 5 mA/cm², respectively. As shown at the lower current density (2 mA/cm²) both birnessite and copper(I)−birnessite show good stability over the time period of the experiment (3000 s). When the measurement is performed at the higher current density (5 mA/cm²) Cu-free birnessite exhibits a comparatively poor stability, evidenced by the experimental observation that to maintain a current density of 5 mA/cm² the potential needs to be increased to 1 V in the first 320 s. In the case of copper(I)−birnessite, the current density can be maintained at 5 mA/cm² for 1100 s before the potential reaches 1 V. We analyzed the catalyst using XPS before and after the electrochemical deactivation (SI Figure S10), and results show that there is still a significant amount of Cu left after the catalysis shows deactivation. Hence Cu loss may not be responsible for the deactivation. We point out that a change in the structure of the birnessite catalyst during electrocatalysis likely contributes to the deactivation as it probably does in the Cu-free birnessite. Future studies will also address this possibility.

Charge transfer kinetics play a key role in electrochemical catalysis where an efficient catalyst should transport charge with low resistance.[30] Electrochemical impedance spectroscopy (EIS) serves as the technique of choice to evaluate the charge transfer resistance in electrochemical catalysts. In a typical Nyquist plot, the low frequency area is useful to evaluate the
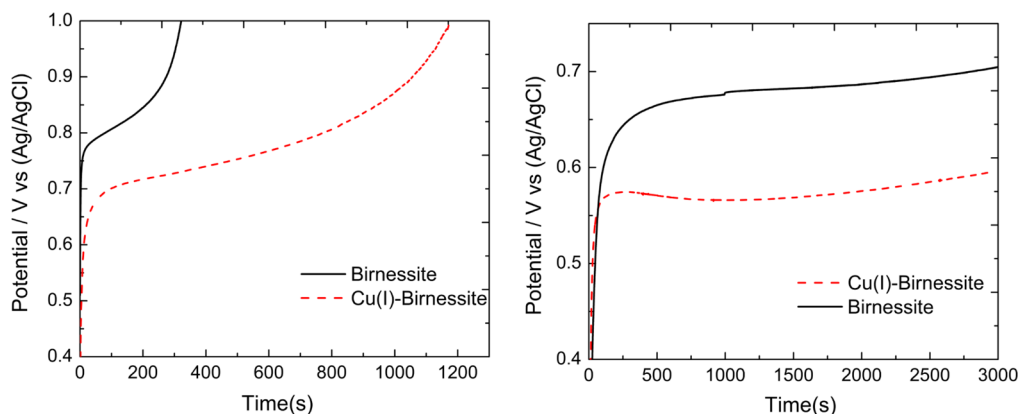

Figure 6. Chronopotentiometry curves for birnessite and copper(I)−birnessite at current densities of 2 mA/cm² (left panel) and 5 mA/cm² (right panel).

charge transfer resistance between electrolyte and catalytic surface, whereas the high frequency area is capable of providing information about charge transfer resistance between the catalytic surface and reactants.[30] The obtained Nyquist plots for birnessite and the Cu-modified birnessite materials used in this study are shown in Figure 7. Charge transfer resistances
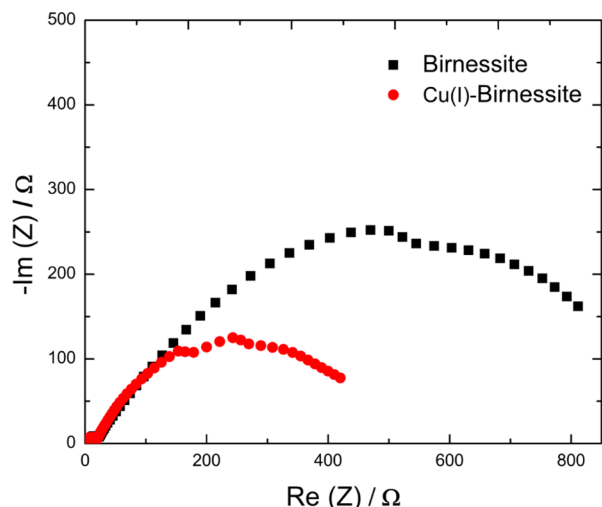

Figure 7. Nyquist plot obtained from EIS measurement at an applied potential of 0.65 V (vs Ag/AgCl) for pristine birnessite and copper(I)−birnessite.

were obtained from fitted equivalent circuits (SI Table S1). The observed charge transfer resistance of 680 Ω for birnessite agrees well with values reported in the literature.[4] Consistent with our DFT calculation that the intercalation of Cu into the birnessite interlayer increases the conductivity of the material, we find a charge transfer resistance of 472 Ω for copper(I)−birnessite, significantly lower than for birnessite. The impedance spectra for carbon black alone, which is used to increase the conductivity of the birnessite samples on the working electrode, showed a charge transfer resistance of about 3000 Ω. Hence, carbon black is a good electrical conductor but poor catalyst for water oxidation as evidenced by the high charge transfer resistance (SI Figure S8).

Interpretation of the experimental results in view of the DFT calculations suggest that one role of the interlayer Cu is to lower the charge transfer resistance of the catalyst. In short, the realization from calculation that Cu intercalation leads to filled electron states at the Fermi level of copper(I)−birnessite would be consistent with the lower resistance for charge transfer. The increase in the stability of birnessite when Cu is in the interlayer could also be due to an improvement in charge conductivity between sheets (out-of-plane). Such a change in the electrical properties of birnessite with interlayer Cu might allow more sheets to be active for electrocatalytic water oxidation. We cannot rule out, however, that other effects play a role in the enhancement due to Cu. As mentioned before, redox chemistry between interlayer Cu^0 and Mn(IV) could lead to the production of Mn(III), a species that has been shown in other studies to be particularly important for enhancing water oxidation on manganese oxides.[17,18,31] The relatively low concentration of Cu in the interlayer (<4%) suggests that the maximum amount of Mn(III) that could be formed from the interaction of Cu^0 and Mn(IV) (~4% increase in Mn(III)) would be too low to be responsible for our experimental

observations. Also, there is a small contraction in the interlayer distance of copper(I)−birnessite when compared to birnessite. It is plausible that the reduced spacing leads to enhanced water oxidation in the interlayer region, and it would be an interesting area of future investigation.

It is informative to compare the properties of copper(I)−birnessite to α-MnO_2, which has been shown to be the manganese oxide with the most attractive electrocatalytic properties for the oxygen evolution reaction. Unlike birnessite, the structure of α-MnO_2 is a manganese octahedral molecular sieve with the Mn having both +3 and +4 oxidation states.[32] This particular material has been shown to exhibit an overpotential for water oxidation of ~500 mV with a stability that is much greater than birnessite.[4] In particular, at a current density of 5 mA, α-MnO_2 can maintain a relatively stable overpotential (after reaching 0.8 V) for water oxidation for ~3 h ($\Delta\eta$ = 0.2 V after 3 h), while the stability time for birnessite is ~5 min for the same current density and similar overpotential increase. We showed in this contribution that modification of birnessite via the intercalation of Cu into its interlayer region results in a lowering of the overpotential (from >0.7 to 0.49 V) to a value similar to α-MnO_2 and the stability time for a current density of 5 mA/cm^2 increased to 20 min (compared to 5 min for Cu-free birnessite). Hence, these studies show that the electrocatalytic behavior of birnessite can be improved through the judicious use of intercalated atoms. Studies are underway to further improve the catalytic reactivity of birnessite by changing the metal center as well as the intercalated metal concentration.

4. SUMMARY

A strategy to enhance the catalytic activity toward water oxidation in layered manganese oxide has been realized by introducing Cu within the interlayers. Both XRD and Raman spectroscopy measurements support the presence of Cu in the interlayer of birnessite. XPS results suggest that a portion of Cu that enters the interlayer remains as Cu^0 and another significant fraction of Cu exists as Cu^{2+} in the interlayer, likely resulting from the oxidation of Cu^0. DFT calculations suggest that the introduction of Cu^0 into the interlayer results in a change in the electrical properties of birnessite from a semiconductor to metal. Consistent with calculation, electrochemical impedance measurements acquired during water oxidation reaction show that the charge transfer resistance of copper(I)−birnessite is lower than birnessite. Perhaps, more importantly, the TOF for water oxidation increases by a factor of ~6 when Cu is present in the birnessite interlayer. We anticipate that these results will have broad utility in devising strategies for improving the catalytic activity of layered materials with intercalated metals.

■ ASSOCIATED CONTENT

Ⓢ Supporting Information

The Supporting Information is available free of charge on the ACS Publications website at DOI: 10.1021/acs.langmuir.5b02936.

> Images of optimized geometries of birnessite and calculated geometries and images of density of states, XPS, Tafel plots, STEM and EDS mapping, circuit used to obtain charge transfer resistance, Nyquist plot, Raman spectra, and XRD patterns (PDF)

■ AUTHOR INFORMATION

Corresponding Author
*E-mail: dstrongi@temple.edu.

Notes
The authors declare no competing financial interest.

■ REFERENCES

(1) Hurst, J. K. In Pursuit of Water Oxidation Catalysts for Solar Fuel Production. *Science* **2010**, *328* (5976), 315−316.

(2) Lewis, N. S.; Nocera, D. G. Powering the planet: Chemical challenges in solar energy utilization. *Proc. Natl. Acad. Sci. U. S. A.* **2006**, *103* (43), 15729−15735.

(3) Kanan, M. W.; Nocera, D. G. In Situ Formation of an Oxygen-Evolving Catalyst in Neutral Water Containing Phosphate and Co^{2+}. *Science* **2008**, *321* (5892), 1072−1075.

(4) Meng, Y.; Song, W.; Huang, H.; Ren, Z.; Chen, S.-Y.; Suib, S. L. Structure−Property Relationship of Bifunctional MnO_2 Nanostructures: Highly Efficient, Ultra-Stable Electrochemical Water Oxidation and Oxygen Reduction Reaction Catalysts Identified in Alkaline Media. *J. Am. Chem. Soc.* **2014**, *136* (32), 11452−11464.

(5) McAlpin, J. G.; Stich, T. A.; Casey, W. H.; Britt, R. D. Comparison of cobalt and manganese in the chemistry of water oxidation. *Coord. Chem. Rev.* **2012**, *256* (21−22), 2445−2452.

(6) Singh, A.; Spiccia, L. Water oxidation catalysts based on abundant 1st row transition metals. *Coord. Chem. Rev.* **2013**, *257* (17−18), 2607−2622.

(7) Subbaraman, R.; Tripkovic, D.; Chang, K.-C.; Strmcnik, D.; Paulikas, A. P.; Hirunsit, P.; Chan, M.; Greeley, J.; Stamenkovic, V.; Markovic, N. M. Trends in activity for the water electrolyser reactions on 3d M(Ni,Co,Fe,Mn) hydr(oxy)oxide catalysts. *Nat. Mater.* **2012**, *11* (6), 550−557.

(8) Gao, M.-R.; Xu, Y.-F.; Jiang, J.; Yu, S.-H. Nanostructured metal chalcogenides: synthesis, modification, and applications in energy conversion and storage devices. *Chem. Soc. Rev.* **2013**, *42* (7), 2986−3017.

(9) Liang, L.; Cheng, H.; Lei, F.; Han, J.; Gao, S.; Wang, C.; Sun, Y.; Qamar, S.; Wei, S.; Xie, Y. Metallic Single-Unit-Cell Orthorhombic Cobalt Diselenide Atomic Layers: Robust Water-Electrolysis Catalysts. *Angew. Chem., Int. Ed.* **2015**, *54*, 12004−12008.

(10) Kanan, M. W.; Surendranath, Y.; Nocera, D. G. Cobalt-phosphate oxygen-evolving compound. *Chem. Soc. Rev.* **2009**, *38* (1), 109−114.

(11) Suntivich, J.; May, K. J.; Gasteiger, H. A.; Goodenough, J. B.; Shao-Horn, Y. A Perovskite Oxide Optimized for Oxygen Evolution Catalysis from Molecular Orbital Principles. *Science* **2011**, *334* (6061), 1383−1385.

(12) Umena, Y.; Kawakami, K.; Shen, J.-R.; Kamiya, N. Crystal structure of oxygen-evolving photosystem II at a resolution of 1.9[thinsp]A. *Nature* **2011**, *473* (7345), 55−60.

(13) Gorlin, Y.; Jaramillo, T. F. A Bifunctional Nonprecious Metal Catalyst for Oxygen Reduction and Water Oxidation. *J. Am. Chem. Soc.* **2010**, *132* (39), 13612−13614.

(14) Wei, J.; Liu, Y.; Ding, Y.; Luo, C.; Du, X.; Lin, J. MnO_2 spontaneously coated on carbon nanotubes for enhanced water oxidation. *Chem. Commun.* **2014**, *50* (80), 11938−11941.

(15) Klápště, B.; Vondrák, J.; Velická, J. MnO_x/C composites as electrode materials II. Reduction of oxygen on bifunctional catalysts based on manganese oxides. *Electrochim. Acta* **2002**, *47* (15), 2365−2369.

(16) Menezes, P. W.; Indra, A.; Levy, O.; Kailasam, K.; Gutkin, V.; Pfrommer, J.; Driess, M. Using nickel manganese oxide catalysts for efficient water oxidation. *Chem. Commun.* **2015**, *51* (24), 5005−5008.

(17) Indra, A.; Menezes, P. W.; Schuster, F.; Driess, M., Significant role of Mn(III) sites in eg1 configuration in manganese oxide catalysts for efficient artificial water oxidation. *J. Photochem. Photobiol., B* **2015**, DOI: 10.1016/j.jphotobiol.2014.11.012

(18) Pickrahn, K. L.; Park, S. W.; Gorlin, Y.; Lee, H.-B.-R.; Jaramillo, T. F.; Bent, S. F. Active MnOx Electrocatalysts Prepared by Atomic Layer Deposition for Oxygen Evolution and Oxygen Reduction Reactions. *Adv. Energy Mater.* **2012**, *2* (10), 1269−1277.

(19) Zaharieva, I.; Chernev, P.; Risch, M.; Klingan, K.; Kohlhoff, M.; Fischer, A.; Dau, H. Electrosynthesis, functional, and structural characterization of a water-oxidizing manganese oxide. *Energy Environ. Sci.* **2012**, *5* (5), 7081−7089.

(20) Robinson, D. M.; Go, Y. B.; Mui, M.; Gardner, G.; Zhang, Z.; Mastrogiovanni, D.; Garfunkel, E.; Li, J.; Greenblatt, M.; Dismukes, G. C. Photochemical Water Oxidation by Crystalline Polymorphs of Manganese Oxides: Structural Requirements for Catalysis. *J. Am. Chem. Soc.* **2013**, *135* (9), 3494−3501.

(21) Kuo, C.-H.; Mosa, I. M.; Poyraz, A. S.; Biswas, S.; El-Sawy, A. M.; Song, W.; Luo, Z.; Chen, S.-Y.; Rusling, J. F.; He, J.; Suib, S. L. Robust Mesoporous Manganese Oxide Catalysts for Water Oxidation. *ACS Catal.* **2015**, *5* (3), 1693−1699.

(22) Motter, J. P.; Koski, K. J.; Cui, Y. General Strategy for Zero-Valent Intercalation into Two-Dimensional Layered Nanomaterials. *Chem. Mater.* **2014**, *26* (7), 2313−2317.

(23) McKenzie, R. M. The synthesis of birnessite, cryptomelane, and some other oxides and hydroxides of manganese. *Mineral. Mag.* **1971**, *38* (296), 493−502.

(24) Villalobos, M.; Toner, B.; Bargar, J.; Sposito, G. Characterization of the manganese oxide produced by pseudomonas putida strain MnB1. *Geochim. Cosmochim. Acta* **2003**, *67* (14), 2649−2662.

(25) Kresse, G.; Joubert, D. From ultrasoft pseudopotentials to the projector augmented-wave method. *Phys. Rev. B: Condens. Matter Mater. Phys.* **1999**, *59* (3), 1758−1775.

(26) Sun, J.; Ruzsinszky, A.; Perdew, J. P. Strongly Constrained and Appropriately Normed Semilocal Density Functional. *Phys. Rev. Lett.* **2015**, *115* (3), 036402.

(27) Koski, K. J.; Cha, J. J.; Reed, B. W.; Wessells, C. D.; Kong, D.; Cui, Y. High-Density Chemical Intercalation of Zero-Valent Copper into Bi2Se3 Nanoribbons. *J. Am. Chem. Soc.* **2012**, *134* (18), 7584−7587.

(28) Koski, K. J.; Wessells, C. D.; Reed, B. W.; Cha, J. J.; Kong, D.; Cui, Y. Chemical Intercalation of Zerovalent Metals into 2D Layered Bi2Se3 Nanoribbons. *J. Am. Chem. Soc.* **2012**, *134* (33), 13773−13779.

(29) Julien, C.; Massot, M.; Baddour-Hadjean, R.; Franger, S.; Bach, S.; Pereira-Ramos, J. P. Raman spectra of birnessite manganese dioxides. *Solid State Ionics* **2003**, *159* (3−4), 345−356.

(30) He, Z.; Mansfeld, F. Exploring the use of electrochemical impedance spectroscopy (EIS) in microbial fuel cell studies. *Energy Environ. Sci.* **2009**, *2* (2), 215−219.

(31) McKendry, I. G.; Kondaveeti, S. K.; Shumlas, S. L.; Strongin, D. R.; Zdilla, M. J. Decoration of the layered manganese oxide birnessite with Mn(ii/iii) gives a new water oxidation catalyst with fifty-fold turnover number enhancement. *Dalton Transactions* **2015**, *44* (29), 12981−12984.

(32) Cai, J.; Liu, J.; Willis, W. S.; Suib, S. L. Framework Doping of Iron in Tunnel Structure Cryptomelane. *Chem. Mater.* **2001**, *13* (7), 2413−2422.